

A deep graph model for the signed interaction prediction in biological network

Shuyi Jin^{1†}, Mengji Zhang^{2†}, Meijie Wang³, Lun Yu^{3*}

^{1*}Department of Biomedical Informatics, National University of Singapore, 119077, Singapore.

²Shanghai Fosun Pharmaceutical (Group) Co., Ltd., Shanghai, 200233, China.

³Metanovas Biotech, Inc., San Francisco, 94108, CA, USA.

*Corresponding author(s). E-mail(s): lunyu@metanovas.com;

Contributing authors: caesarhhh628@gmail.com;

mengji.zhang0809@gmail.com;

[†]These authors contributed equally to this work.

Abstract

Predicting signed interactions in biological networks is crucial for understanding drug mechanisms and facilitating drug repurposing. While deep graph models have demonstrated success in modeling complex biological systems, existing approaches often fail to distinguish between positive and negative interactions, limiting their utility for precise pharmacological predictions. In this study, we propose a novel deep graph model, RGCNTD (Relational Graph Convolutional Network with Tensor Decomposition), designed to predict both polar (e.g., activation, inhibition) and non-polar (e.g., binding, affect) chemical-gene interactions. Our model integrates graph convolutional networks with tensor decomposition to enhance feature representation and incorporates a conflict-aware sampling strategy to resolve polarity ambiguities. We introduce new evaluation metrics, $AUC_{polarity}$ and $CP@500$, to assess the model’s ability to differentiate interaction types. Experimental results demonstrate that RGCNTD outperforms baseline models, achieving superior classification accuracy and improved discrimination of polar edges. Furthermore, we analyze the impact of subgraph components on predictive performance, revealing that additional network structures do not always enhance accuracy. These findings highlight the importance of polarity-aware modeling in drug discovery and network pharmacology, providing a robust framework for predicting complex biological interactions.

Keywords: deep graph model, signed network, chemical-gene interaction, network pharmacology

1 Introduction

In the new era of pharmaceutical research and development, the drug repurposing strategy plays a particularly critical role in exploring innovative therapies. This approach, through the rediscovery of existing drugs for new pathways or diseases, not only accelerates the pace at which new drugs reach the market but also significantly reduces the resource and time costs involved in the research and development process[1]. For instance, doxycycline, a broad-spectrum antibiotic, was rapidly applied in clinical settings during the COVID-19 outbreak through drug repurposing, enhancing public health response efficiency and achieving notable results[2]. Thalidomide, once banned for its teratogenic effects, has been repurposed for treating multiple myeloma and other cancers, reducing drug development costs and improving patient survival rates[3]. Meanwhile, network pharmacology has provided a theoretical basis for identifying new drug indications by constructing and analyzing the interaction networks between drugs and their biological targets[4]. For example, the use of network pharmacology methods to analyze the interactions between known drugs and disease-related targets, thereby discovering the drugs’ potential new indications[5], or by analyzing the interaction networks between drug components to optimize drug combinations, enhancing therapeutic effects and reducing side effects. This method is significant for the treatment of complex diseases[6]. With the rapid development of bioinformatics and computational biology, there has been an increasing integration of advanced computational techniques such as deep graph models. These models are proving to be powerful tools in biomedical network analysis, thanks to their efficiency and accuracy in capturing complex network relationships, thus offering new insights into network pharmacology strategies[7].

Deep graph models have brought revolutionary progress in the exploration of drug repurposing, particularly in the detailed revelation of chemical-gene interactions[8, 9]. Gaudelet et al. [10] explored the use of graph machine learning, including Graph Attention Networks (GATs), to predict drug-target interactions, offering new strategies for drug discovery. Zitnik et al. [11] used Graph Convolutional Networks (GCNs) to predict potential side effects of drug combinations, effectively enhancing the safety evaluation of polypharmacy by analyzing drug-drug interaction networks. Liang et al. [12] utilized GCNs to analyze the Drug-Gene Interaction database (DGIdb), showcasing the potential applications of GCNs in drug repurposing. However, despite their great performances, existing models still face several critical limitations. Models often fail to consider the sign of edges in the network[13, 14], such as whether the mechanism of actions by a drug is stimulatory or inhibitory. For example, in the DrugBank database, the relations between drugs and targets could be polar. Relations such as ‘agonist’, ‘activator’, and ‘inducer’ indicate positive effects of the drug, whereas ‘inhibitor’, ‘blocker’, and ‘antagonist’ suggest negative effects. Often, terms like ‘affect’

are also used, merely indicating an interaction. These nuances in biological significance are frequently ignored in unsigned networks as models struggle to differentiate between labels that signify positive, negative, or neutral effects. The sign of edges (or polar edges/relations) is crucial for a deep understanding and accurate prediction of complex interactions within biological networks. The introduction of signed networks in protein-protein interaction network edge prediction by Mason et al.[15] and in gene co-expression networks by Kuhn et al.[16] has achieved significant success. Previous research has proven that constructing signed networks and using graph convolutional neural networks for predicting interactions between biological entities can achieve excellent results. Teams led by Yang [17] and Chen[18] achieved notable outcomes in protein-protein interaction data and drug-drug interaction data, respectively. However, incorporating the mechanism of actions by chemicals into the networks has not yet been studied.

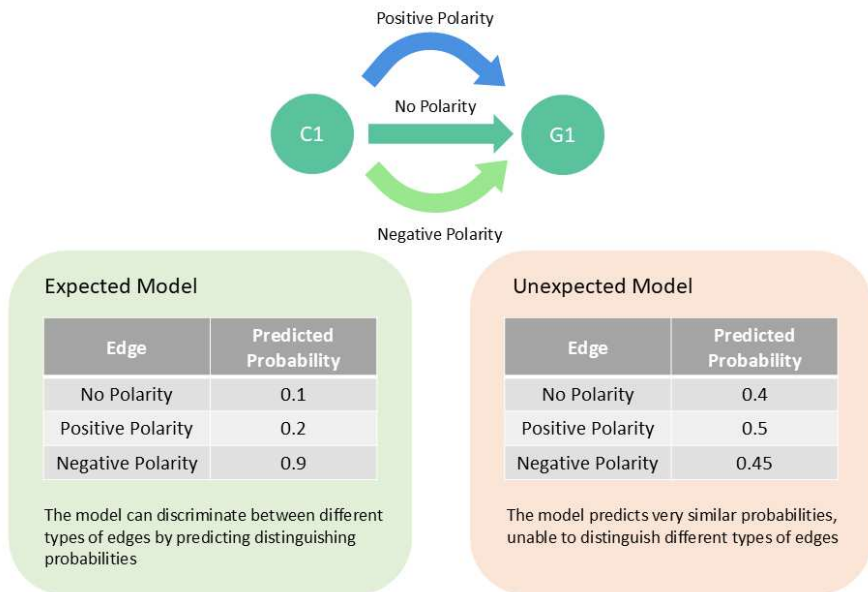


Fig. 1 To model a triplet pair within the network, the edges could be polar (e.g., positive or negative) or non-polar (e.g., neutral). In cases where polarity is present, the model is expected to accurately distinguish and identify the edge’s polarity.

In modeling chemical-gene interaction networks, the current prediction models are designed solely for predicting interaction types without considering the polarity of these relationships. Additionally, they have not been trained to differentiate between polar and non-polar edges. We expect the model to exhibit a more significant probability difference for opposite polarities, as the model can discriminate between different types of edges by predicting distinguishing probabilities. In contrast, we do not anticipate models that predict very similar probabilities across various polarities, which

are unable to distinguish between different types of edges (Fig.1). Although signed networks have been proposed as a solution to address polarity, these networks cannot accommodate the presence of non-polar edges (such as ‘binding’ or ‘affect’). This limitation highlights the need for models that can handle both polar and non-polar edges in a unified framework. To address these challenges, we have taken several innovative strategies. First, we developed a sophisticated deep graph model capable of handling signed networks. It not only addresses the limitation of existing methods that often ignore the polarity of the network but is also compatible with non-polar relations[19]. In our model, the network contains polar relations (e.g., activation and inhibition) that are mutually exclusive to each other, and it also contains non-polar relations (e.g., binding) that could be co-existent. By identifying these complex and multifaceted relationships, our model provides a more detailed and dynamic perspective on chemical-gene interactions. We also implemented new evaluation metrics for the chemical-gene interaction network. Such metrics have been demonstrated to significantly improve the consistency and accuracy of model evaluations[20]. At last, we conducted a thorough analysis of the characteristics of different components within the network and their impact on model performance. Based on this analysis, we proposed a series of strategies to optimize the model’s predictive capabilities. These strategies include data preprocessing, model structure optimization, and negative sampling during the training process, collectively aimed at enhancing the model’s accuracy and reliability.

2 Results

2.1 Performance Of Models Prediction

In this study, we designed and implemented a novel decoder model that integrates Relational Graph Convolutional Networks with tensor decomposition (RGCNTD), to enhance the accuracy of predicting chemical-gene interactions. We utilized several widely recognized classification metrics to comprehensively evaluate the model’s performance, including macro AUROC, micro AUROC, macro AUPRC, micro AUPRC, and the average precision of the top 20 predictions (AP@20). Leveraging the encoder framework provided by BioNet[21], we compared the performance of the original BioNet model with our RGCNTD model to validate its improvements. The results demonstrate that RGCNTD outperformed BioNet across all evaluation metrics, showcasing superior classification capability, enhanced robustness, and improved adaptability to imbalanced datasets.

Specifically, the RGCNTD model achieved scores of 0.966 and 0.980 in macro AUROC and micro AUROC, respectively, significantly surpassing the corresponding scores of 0.939 and 0.959 achieved by BioNet. This indicates a substantial improvement in both overall classification performance and the classification across all classes. In terms of macro AUPRC and micro AUPRC, the RGCNTD model attained scores of 0.961 and 0.971, respectively, further highlighting its superior handling of imbalanced data, particularly in identifying positive samples from minority classes. Moreover, the RGCNTD model excelled in the AP@20 metric, achieving a score of 0.968, a significant improvement over BioNet’s 0.824, demonstrating marked advancements

in accuracy for the top 20 predictions. These results validate the RGCNTD model’s exceptional performance in predicting chemical-gene interactions.

To further substantiate the effectiveness of the RGCNTD model, we conducted a comparative analysis against several mainstream models (Table 1), including RGCN, GraphSAGE, and TransE. The results demonstrate that the RGCNTD model outperformed these alternatives across all metrics. The RGCN model achieved macro AUROC and micro AUROC scores of 0.530 and 0.572, respectively, reflecting significant limitations in overall classification performance and adaptability to class imbalance. GraphSAGE exhibited an even weaker performance, with a micro AUROC score of only 0.541. Although TransE showed marginally better performance than RGCN and GraphSAGE, its AUROC and AUPRC scores remained below 0.6, falling considerably short of the RGCNTD model. In the AP@20 metric, the RGCNTD model excelled with a score of 0.968, far surpassing the scores of 0.376 and 0.367 achieved by RGCN and GraphSAGE, respectively, which rendered their performance almost impractical for real-world applications.

Table 1 Model Performance Metrics

Prediction	MACRO_AUROC	MICRO_AUROC	MACRO_AUPRC	MICRO_AUPRC	AP@20
RGCNTD	0.966	0.980	0.961	0.971	0.968
BioNet	0.939	0.959	0.925	0.937	0.824
RGCN	0.530	0.572	0.530	0.509	0.376
GraphSAGE	0.531	0.541	0.450	0.489	0.367
TransE	0.553	0.556	0.599	0.610	0.489

2.2 Conflicting Edge Sampling Strategy

In our study, ‘edge conflicts’ specifically refer to the conflicts during polarity predictions by the model, such as the same sample being predicted as both ‘activation’ and ‘inhibition’. To avoid such conflicts, the model has to accurately distinguish between polar edges, such as activation and inhibition, which is crucial for understanding and predicting network behavior.

We analyzed the conflicting predictions among RGCNTD, RGCN, GraphSAGE, and TransE models by examining the paired line plots shown in Fig.2 illustrate the performance of the four models in polar edge analysis. The left side of each figure represents ‘Decrease’ interactions, while the right side represents ‘Increase’ interactions. The lines connecting the log2-transformed rankings show how well the models distinguish between the two types of interactions. From these figures, we can observe that the RGCNTD (Fig.2 A) has the smallest overlap between the left and right sides, indicating its strong ability to differentiate edge polarity. However, there are still noticeable cases of polarity conflicts in its predictions. In contrast, the RGCN and the TransE models show more significant overlapping regions, highlighting the limitations of these models in distinguishing edge polarity, with conflicting predictions remaining

widespread. The GraphSAGE model performs the worst in this regard, with almost complete overlap between the left and right sides, indicating its inability to distinguish between ‘Increase’ and ‘Decrease’ interactions effectively.

By introducing the Cannot-Link (CL) conflicting edge sampling strategy, our model demonstrates enhanced discriminative capabilities when handling data with polar edges, significantly improving the accuracy in identifying polar relationships. After introducing the conflict sampling strategy (CL sampling), we re-evaluated several models and observed performance improvements across various metrics (Table 2). Table 2 illustrates the performance differences of various models before and after introducing the CL sampling strategy. After applying CL sampling, the RGCNTD-CL showed significant improvements, with AUROC increasing from 0.966 to 0.985, AUPRC rising from 0.961 to 0.975, and AP@20 achieving a perfect score of 1. These results demonstrate that the CL sampling strategy greatly enhanced the generalization ability and accuracy of the RGCNTD model in recognizing complex interactions. For other baseline models, improvements were also observed with CL sampling, though not as pronounced as those for the RGCNTD model. RGCN-CL exhibited improvements in AP@20, which increased from 0.376 to 0.421, although AUROC declined from 0.530 to 0.509. GraphSAGE-CL showed more noticeable improvements, with macro AUROC increasing from 0.531 to 0.550 and AP@20 rising from 0.367 to 0.437, suggesting that the CL sampling strategy enhanced its performance. TransE-CL displayed slight improvements, with macro AUROC increasing from 0.553 to 0.573 and AP@20 rising from 0.489 to 0.510. Overall, the CL sampling strategy had the most significant impact on the RGCNTD model, while the improvements for other baseline models were also noticeable.

Table 2 Model Performance Metrics with and without CL

Model	MACRO_AUROC	MICRO_AUROC	MACRO_AUPRC	MICRO_AUPRC	AP@20
RGCNTD	0.966	0.980	0.961	0.971	0.968
RGCNTD-CL	0.985	0.980	0.975	0.974	1
RGCN	0.530	0.572	0.530	0.509	0.376
RGCN-CL	0.509	0.547	0.533	0.512	0.421
GraphSAGE	0.531	0.541	0.450	0.489	0.367
GraphSAGE-CL	0.550	0.553	0.477	0.493	0.437
TransE	0.553	0.556	0.599	0.610	0.489
TransE-CL	0.573	0.569	0.599	0.611	0.510

The impact of the CL sampling strategy on the model’s ability to distinguish polarity can be observed using the paired line plot in Fig.2. This plot visualizes the ranking of predictions for a pair of entities corresponding to ‘Increase’ and ‘Decrease’ polarity, allowing us to assess how effectively the model differentiates between them. For a given pair of entities, a well-performing model should assign distinctly different ranks to ‘Increase’ and ‘Decrease’. This means that in the paired line plot, a larger gap between the two ranks indicates better model performance. We compared our models with the baseline models. For the RGCNTD model (Fig.2 A), the overlapping region between

the left and right sides significantly decreased, indicating that the CL sampling strategy effectively enhanced the model’s ability to differentiate between "Increase" and "Decrease" interactions, and significantly reduced edge conflicts. The RGCN model (Fig.2 B) and the TransE model (Fig.2 C) also showed improvements after the introduction of CL sampling, although conflicting regions remained relatively visible. The GraphSAGE model (Fig.2 D) exhibited the most significant improvement among all baseline models, with a substantial reduction in the overlap between the two sides, reflecting a marked enhancement in polarity distinction. Overall, the CL sampling strategy improved the ability to distinguish edge polarity across all models, with the RGCNTD model benefiting the most. This demonstrates the effectiveness of the strategy in addressing edge conflict issues.

2.3 Designed Metrics for Polairty Prediction

By evaluating two custom metrics (Table 3), AUC_polarity and CP@500, we could more accurately capture the models’ performance in polarity edge and high-confidence predictions. The results demonstrate that the conflict sampling strategy (CL sampling) brought significant improvements, especially for our model. After introducing CL sampling, the RGCNTD model’s AUC_polarity increased from 0.378 to 0.696, and CP@500 rose from 0.762 to 0.866. These improvements indicate that CL sampling greatly enhanced the model’s ability to differentiate edge polarity and more accurately predict interactions. These two metrics effectively validate the positive impact of CL sampling on handling complex interactions. For baseline models such as RGCN, GraphSAGE, and TransE, although CL sampling also improved AUC_polarity and CP@500, the effects were not as pronounced as with our model. For instance, RGCN’s AUC_polarity increased from 0.256 to 0.327, and CP@500 improved from 0.237 to 0.471, while the improvements for GraphSAGE and TransE were similarly limited. Despite some improvements in handling polarity conflicts with the help of CL sampling, the limited capacity of these baseline models restricted the extent of improvement.

This result suggests that our custom metrics, AUC_polarity and CP@500, effectively evaluate model performance in polarity prediction scenarios. Not only do they confirm the effectiveness of the CL sampling strategy, but they also highlight the significant advantage of the RGCNTD model in addressing complex interactions and polarity edge prediction.

This result suggests that our custom metrics, AUC_polarity and CP@500, effectively evaluate model performance in polarity prediction scenarios. Not only do they confirm the effectiveness of the CL sampling strategy, but they also highlight the significant advantage of the RGCNTD model in addressing complex interactions and polarity edge prediction.

2.4 Impact of Network Component

Besides chemical-gene interaction networks, we also explored introducing subgraph structures (only chemical-chemical subgraphs, gene-gene subgraphs, and both) for

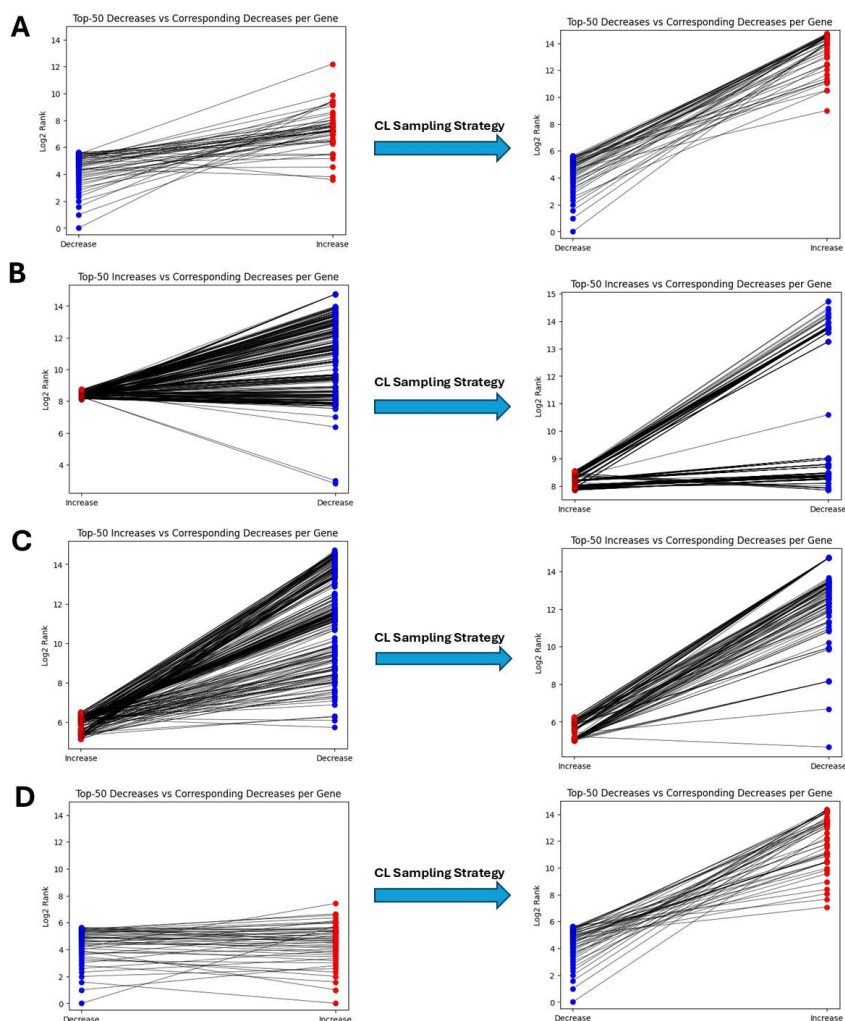


Fig. 2 The figures illustrate the performance of four models (RGCNTD, RGCN, GraphSAGE, and TransE) in polarity edge analysis. The left-side plots show the models' performance without the CL sampling strategy, while the right-side plots display results after incorporating the strategy. The log₂-transformed ranking lines connecting the two sides highlight each model's ability to differentiate between the two types of interactions

training to understand their potential impact on the predictive performance of chemical-gene interactions. We discovered that, in some instances, adding subgraph structures could harm model performance (Table 4). Without the introduction of sub-graph structures (No Subgraph), the model achieved its best performance across all metrics, with macro AUROC and micro AUROC reaching 0.985 and 0.980, respectively, macro AUPRC and micro AUPRC at 0.975 and 0.974, and AP@20 at 1. Additionally, the two custom metrics, AUC_polarity and CP@500, scored 0.696 and

Table 3 AUC Polarity and CP@500 Metrics

Model	AUC_{polarity}	CP@500
RGCNTD	0.378	0.762
RGCNTD-CL	0.696	0.866
RGCN	0.256	0.237
RGCN-CL	0.327	0.471
GraphSAGE	0.212	0.218
GraphSAGE-CL	0.378	0.451
TransE	0.102	0.152
TransE-CL	0.410	0.479

0.866, respectively, demonstrating the model’s exceptional classification ability and prioritization performance. In contrast, when subgraph structures were introduced (Subgraph), the model’s performance significantly declined, with macro AUROC and micro AUROC dropping to 0.839 and 0.877, macro AUPRC and micro AUPRC reducing to 0.825 and 0.851, and AP@20 falling to 0.781. Furthermore, the metrics AUC_{polarity} and CP@500 also decreased to 0.521 and 0.771, respectively, indicating that the RGCNTD model is better suited for data structures without subgraphs.

Table 4 Comparison of Model Performance Before and After Using the Chemical-Chemical and Gene-Gene subgraph

Prediction	MACRO_AUROC	MICRO_AUROC	MACRO_AUPRC	MICRO_AUPRC	AP@20	AUC_{polarity}	CP@500
Subgraph	0.839	0.877	0.825	0.851	0.781	0.521	0.771
Only Chemical	0.948	0.933	0.938	0.927	0.836	0.546	0.972
Only Gene	0.917	0.910	0.882	0.891	0.697	0.557	0.810
No Subgraph	0.985	0.980	0.975	0.974	1	0.695	0.866

This result highlights the independence and efficiency of the RGCNTD model in processing chemical-gene interaction data. It indicates that for the specific dataset, the RGCNTD model has been optimized to a point where introducing subgraph structures not only fails to enhance predictive performance but may even reduce it due to the introduction of unnecessary complexity. Our study underscores the importance of developing models tailored to a dataset’s specific needs and provides practical guidance on balancing increasing model complexity with maintaining or enhancing performance. Future work will be needed to explore further the relationship between model complexity and predictive performance and how to adjust the model structure for chemical-gene interaction datasets to maximize prediction accuracy.

3 Method

3.1 Model Construction

The RGCNTD model is designed to compute the probability of edge types of interest based on specific node combinations. The model consists of two primary components: the GCN Encoder and the RGCN Tensor Decomposition Decoder. The GCN Encoder

is divided into two layers; the first layer employs a graph convolutional layer to capture the features of the original input data, and the second layer further abstracts these features through another graph convolutional layer to form a more refined representation of the nodes. Subsequently, the RGCN Tensor Decomposition Decoder combines Relational Graph Convolutional Network (RGCN) layers with a DEDICOM tensor decomposition layer, where the former aggregates information according to different relationship types. At the same time, the latter parses global and local interactions, ultimately generating predictions for interactions between entities. As shown in (Fig.3), the model’s architecture fully accounts for the multi-relational nature of graph data, enabling the capture of rich structural information and thus holding extensive application potential in fields such as bioinformatics and recommendation systems.

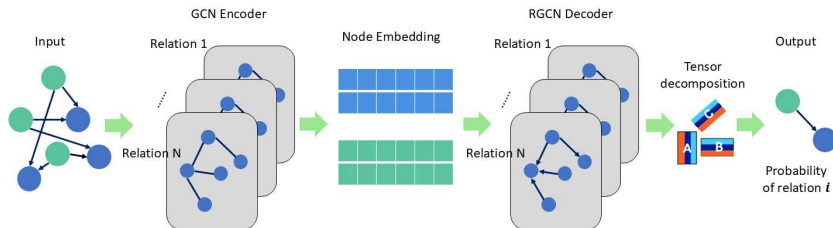


Fig. 3 Overview of model architecture

3.2 Network Construction

In this study, we constructed a network of interactions between chemicals and genes to train models using data from the STITCH database [22]. PubChem CIDs from STITCH were mapped to the ChEBI ID in the ChEBI database [23]. The ChEBI database excludes protein molecules encoded by genes and other insignificant small molecules, focusing solely on chemically meaningful entities. Moreover, ChEBI’s ontology provides a rich structure that facilitates understanding relationships between specific chemical entities and the broader chemical domain [24]. Similarly, protein IDs from STITCH were mapped to NCBI Gene ID.

We also introduced homogeneous graphs, such as the Chemical-Chemical and Gene-Gene interaction networks, to provide the model with additional information and evaluate the impact of complex network inputs on predictive performance. The Gene-Gene interaction network was derived from 1,307,492 interaction records in the STRING database[25]. Chemical-Chemical interaction data was obtained from 1,770,581 records in the ChEBI database[26]. Relationships were based on polarity into the following categories:

1. **Increase:** The compound exerts an activation effect on gene expression or the activity of gene expression products.
2. **Decrease:** The compound exerts an inhibition effect on gene expression or the activity of gene expression products.

3. **Binding:** The compound binds to the gene expression pathway or the products of gene expression.
4. **Affect:** The compound affects gene expression or the activity of gene expression products, but the effect lacks clear polarity or its mechanism remains unclear.

After data cleaning and removing irrelevant molecules, the resulting heterogeneous Chemical-Gene graph contained 12,537 chemical nodes, 28,432 gene nodes, and 183,3943 interaction records distributed across the four relationship types (Table 5). Within this network, we analyzed pairs exhibiting multiple relationship types. We found that 103,738 pairs of entities have both polar and non-polar relationships.

Table 5 Relations in chemical-gene subgraph

No.	Realtion Name	Number of the edges	Polarity
1	Increase	752,037	Increase Polarity
2	Decrease	667,187	Decrease Polarity
3	Binding	403,915	No Polarity
4	Affect	10,803	No Polarity

3.3 Handling Polar Edges in Chemical-Gene Prediction Tasks

In chemical-gene interaction prediction, our dataset encounters the challenge of handling polar edges. Polar edges refer to instances where a chemical and a gene (e.g., the relationship between e_1 and e_2) can exhibit contradictory effects (e.g., increased vs. decreased expression), typically considered mutually exclusive. To effectively capture and present these conflicting relationships, we designed a dual sampling strategy that incorporates both ‘Must-Link’ (ML) and ‘Cannot-Link’ (CL) constraints. These constraints are defined as Equation(1):

$$\begin{aligned}
 \text{ML} &= \{(e_1, r_{\text{label}}, e_2), (e_1, r_{\text{predict}}, e_2) \mid r_{\text{label}} \in \text{Group}_1, r_{\text{predict}} \in \text{Group}_1\} \\
 \text{CL} &= \{(e_1, r_{\text{label}}, e_2), (e_1, r_{\text{predict}}, e_2) \mid r_{\text{label}} \in \text{Group}_1, r_{\text{predict}} \in \text{Group}'_1\}
 \end{aligned} \tag{1}$$

Here, r_{label} represents the true relationship label, and r_{predict} represents the predicted relationship label by the model. Group_1 and Group'_1 represent opposite types of relationships. For example, if Group_1 represents all relationships associated with ”increases”, then Group'_1 represents the corresponding ”decreases” relationships. These definitions help the model more effectively manage similar or opposing relationship types during training. To reflect these constraints in model training, we designed

the following loss function Equation(2):

$$L = \sum_{(e_1, r_{\text{predict}}, e_2) \in \text{ML}} (1 - S(e_1, r_{\text{predict}}, e_2))^2 + \sum_{(e_1, r_{\text{predict}}, e_2) \in \text{CL}} (S(e_1, r_{\text{predict}}, e_2))^2 \quad (2)$$

In this loss function, the goal of the Must-Link (ML) constraint is to ensure that the score $S(e_1, r_{\text{predict}}, e_2)$ for edges belonging to the same semantic category is close to 1. Conversely, the goal of the Cannot-Link (CL) constraint is to ensure that the score $S(e_1, r_{\text{predict}}, e_2)$ for edges belonging to opposite semantic categories is close to 0. This design enables the model to accurately distinguish between different relationship types during training, effectively handling polar edges and improving the accuracy and reliability of the predictions.

In our implementation, we focused specifically on the polarity information of the ‘Increase’ and ‘Decrease’ relationship types, enhancing the model’s ability to differentiate mutually exclusive interactions. By integrating this mechanism into the training routine, the model could learn more nuanced data representations that capture the complexity of biological systems, where certain relationships are inherently polar. This approach improved the model’s discriminative power, resulting in more accurate and biologically meaningful predictions.

3.4 Baseline

We selected RGCN, GraphSAGE, and TransE as baseline models to compare their performance with our RGCNTD model on the benchmarks. RGCN utilizes relation-specific convolutions to handle multi-relational graphs, making it well-suited for predicting edge labels in multi-relational networks. GraphSAGE, known for its scalability, efficiently processes large graphs through neighbor sampling and feature aggregation. TransE, widely used for knowledge graph embeddings, models relationships via vector translations, providing a useful comparison for evaluating our model’s ability to handle complex edge-node interactions. The model parameters are summarized in Table 6:

Table 6 Model Parameters

No.	Parameter	GraphSAGE	RGCN	TransE
1	grad_norm	1.0	1.0	1.0
2	n_bases	4	4	4
3	learning rate	1e-2	1e-2	1e-2
4	regularization	1e-2	1e-2	1e-2
5	n_epochs	1000000	100000	1000000

3.5 Experimental Setup

All experiments were conducted on a server equipped with an NVIDIA GeForce RTX 3090. The RGCNTD model’s encoder was a two-layer graph convolutional network optimized with Chebyshev polynomials. The Adam optimizer was employed for optimization, with an early stopping mechanism incorporated to prevent overfitting. Early stopping was based on the validation loss, with a patience threshold of 5 epochs. The final model was trained for 50 epochs with a batch size of 8192, and the best model parameters were identified at epoch 48. A test size of 8192 was used, and the test results were recorded. A detailed list of parameters used in the model is provided in Table 7

Table 7 Model Parameters

No.	Parameter	Default	Description
1	epoch	50	Number of epoches
2	hidden_dimensions	[128, 64, 32, 16]	List of hidden dimensions for layers
3	batch_size	8192	Batch size for training
4	test_batch	True	Whether to test the data per batch
5	test_batch_size	8192	Batch size for testing
6	print_step	10	Steps of printing information
7	average_precision_k	20	k for average precision at k

3.6 Metrics Design

In this study, we introduced a range of evaluation metrics to assess the models’ performance comprehensively, besides the Area Under the Receiver Operating Characteristic Curve (AUROC) and Area Under the Precision-Recall Curve (AUPRC) and AP@20. To account for the class imbalance in the samples, we calculated both macro and micro levels for the AUROC and AUPRC metrics. Additionally, we designed two novel metrics to evaluate the model’s ability to distinguish polar edges. These metrics highlight the model’s effectiveness in predicting chemical-gene interactions and offer valuable insights for future research.

3.6.1 Average Precision at Polar Edges

In this study, we introduce a new metric C to assess the ability of predictive models to differentiate between the effects of chemicals on genes, specifically "Increase" and "Decrease" interactions. Specifically, C is defined as the absolute difference between the probabilities of "Increase" and "Decrease" edges predicted by the model by the following Equation(3).

$$C = |P_{\text{increase}} - P_{\text{decrease}}| \tag{3}$$

Here, P_{increase} and P_{decrease} represent the model’s predicted probabilities of a chemical increasing or decreasing a gene’s activity, respectively. This metric quantifies the model’s confidence and capability in distinguishing between these two interaction types. However, the initial distribution of C values is typically long-tailed, reflecting a

degree of uncertainty in the model’s predictions for these interactions. To improve the statistical properties of C and facilitate data analysis and interpretation, we applied a mathematical transformation. This transformation function is monotonically increasing within the range of 0 to 1, ensuring that the original ordering of C values is preserved without altering their relative magnitudes. To standardize the range of C and address its high dynamic range, we employed a natural logarithm function (\ln). This approach compresses the dynamic range of C , resulting in a smoother and more uniform distribution. The transformation also incorporates a scaling constant, such as $2\pi^2$, which can be replaced with other alternatives if needed. The transformation function is specified as Equation(4):

$$C' = \frac{\ln(1 + 2\pi^2 \cdot C)}{\ln(2\pi^2 + 1)} \quad (4)$$

We observed significant changes in the distribution of C before and after the transformation. Before transformation(Fig.4 A), the distribution of C exhibited a long-tailed shape, particularly in the non-CL model. A dense concentration of low C values indicated substantial uncertainty in the model’s ability to distinguish between ‘Increase’ and ‘Decrease’ interactions. The long-tailed nature of the distribution makes visual inspection more difficult, as the frequent occurrence of extreme values obscures meaningful patterns in the data. After transformation (Fig.4 B), the distribution of C improved significantly, especially within the CL model. The transformed distribution showed reduced long-tail effects and display greater symmetry and concentration. This adjustment made the distribution easier to visualize and analyze while preserving the metric’s original properties.

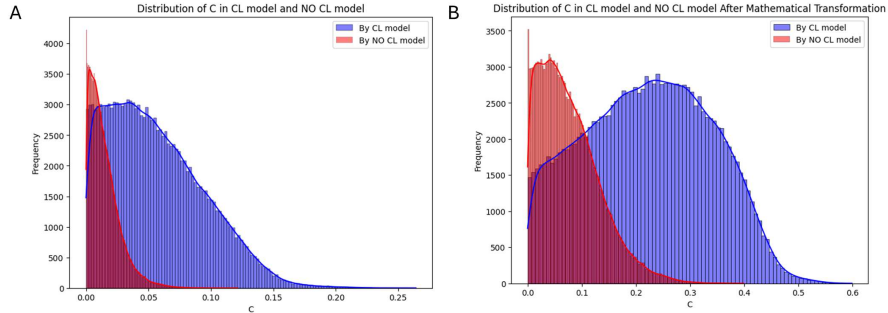


Fig. 4 The distribution of C in the CL model and NO CL model before and after the mathematical transformation.

3.6.2 Polarity Degree (C)-based Precision

To comprehensively assess the model’s performance in high-confidence predictions, we introduce the Polarity Degree (C)-based Precision at 500 (CP@500) metric. This

metric evaluates the model’s accuracy among its top 500 most confident predictions, measuring its precision under high-confidence conditions. The calculation involves the following steps:

1. For each instance in the dataset, we compute the polarity degree (C) as defined in Equation
2. The predictions are then sorted in descending order based on their C value, prioritizing those with the highest confidence (largest C values)
3. Each prediction is evaluated for correctness by comparing the predicted category (the category with larger predicted probability) to the true category. A prediction is marked as correct (1) if the predicted category matches the true category; otherwise, it is marked incorrect (0)
4. Finally, the top k predictions from the sorted list are selected, and the number of correct predictions among these is used to compute CP@k as shown in Equation(5):

$$CP@k = \frac{\text{Number of correct predictions among the top } k}{k} \quad (5)$$

By introducing CP@k, we not only evaluate the model’s accuracy in its most confident predictions, but also emphasize its performance under high-confidence conditions. This metric provides an intuitive and effective way to compare the precision of different models in their top-ranked predictions.

3.6.3 AUC for polar edge

Inspired by the AUC (Area Under the Curve) evaluation methodology, we devised a novel metric called Area Under the Curve for polar edge prediction (AUC_polarity), specifically designed to evaluate the model performance in predicting the polarity (‘Increase’ or ‘Decrease’) of relationships between nodes in a network. To compute AUC_polarity, we randomly select N pairs of nodes connected by edges labeled with ‘Increase’ or ‘Decrease’ polarity. The model predicts the probabilities of ‘Increase’ p_a and ‘Decrease’ p_i , and the task is to determine the actual polarity of each edge based on these probabilities. We utilize a binary indicator \hat{y} . \hat{y} is assigned a value of 1 if the model’s predicted probability of ‘Increase’ is greater than that of ‘Decrease’ and the actual polarity is ‘Increase’. \hat{y} is assigned a value of 0 if the model’s predicted probability of ‘Increase’ is greater than that of ‘Decrease’ and the actual polarity is ‘Decrease’. The metric AUC_polarity is calculated using the Equation(6):

$$AUC_{polarity} = \frac{\sum \text{sign}(p_a - p_i) \times \hat{y}}{N} \quad (6)$$

Here, N is the total number of samples, and $\text{sign}(p_a - p_i)$ calculates the sign of the difference in the predicted probabilities of ‘Increase’ and ‘Decrease’. This metric sensitively reflects the model’s ability to discern polar edges, even in the presence of ambiguous or weak polarity signals.

4 Conclusion

In this study, we introduced a novel deep graph model, RGCNTD (Relational Graph Convolutional Network with Tensor Decomposition), designed to predict signed interactions in biological networks. A key contribution of this work lies in its ability to handle both polar and non-polar edges, which naturally coexist in real-world biological networks. Our dataset revealed multiple types of relationships, with a significant proportion exhibiting polar characteristics, such as ‘Increase’ and ‘Decrease’, while others remained non-polar, reflecting general or undefined interactions. The coexistence of these relations poses unique challenges for predictive models, which our approach effectively addresses.

By incorporating the Conflict-Link (CL) sampling strategy, we enhanced the model’s ability to resolve polarity conflicts and improve high-confidence predictions. Compared to baseline models, RGCNTD demonstrated superior performance, particularly in distinguishing interactions with opposing polarities. The introduction of novel metrics, AUC_polarity and CP@500, was instrumental in evaluating the model’s capability to differentiate between polar and non-polar edges. These metrics provided deeper insights into the model’s predictive power within complex biological networks where diverse relationships coexist and interact.

Modeling such complexity is crucial, as it better reflects the true nature of biological systems, where multiple types of interactions occur simultaneously. This work advances our understanding of drug-gene interactions and emphasizes the importance of polarity-aware modeling in biological research. Accurately distinguishing between interaction types has significant implications for interpreting biological processes and guiding downstream applications.

This study highlights the practical significance of developing models capable of handling diverse relationships, offering a more comprehensive and accurate representation of biological networks. Future research can build on this by exploring improved strategies for resolving conflicting predictions and expanding the application of polarity-aware methods to broader biological and clinical contexts.

5 Ethics Statement

This study does not contain any studies with human participants or animals performed by any of the authors.

6 Data and Code Availability Statement

The dataset and code used in this study are available from the corresponding author upon reasonable request.

7 Appendix

7.0.1 Graph Convolutional Encoder

In this study, we employed a Graph Convolutional Encoder designed to capture and encode the intricate cooperative interactions between chemicals and genes. The graph convolutional encoder utilizes a hierarchical graph convolutional network architecture that iteratively aggregates and propagates information across nodes to learn node embeddings. The input to this architecture is a graph constructed from nodes represented as one-hot vectors and edges represented through adjacency matrices. The encoder opts for a two-layer GCN optimized using Chebyshev polynomials, which has proven to exhibit enhanced performance, as evidenced in previous studies. The feature update for a node v_i is given by Equation(7):

$$h_i^{k+1} = \sigma \left(\sum_{r \in R} \sum_{j \in N_i^r} \frac{1}{\sqrt{|N_i^r| |N_j^r|}} W_r^k h_j^k + \frac{1}{|N_i^r|} h_i^k \right) \quad (7)$$

Here, σ represents a non-linear activation function, N_i^r denotes the neighbors of node v_i with a link type r , and W_r^k signifies the learnable parameter matrix associated with relation type r . This equation is responsible for updating node features by leveraging information from first-order neighbors across different relation types. Progressing to the subsequent stage, the hidden state \tilde{h}_i for each node is computed within the dimensionality of $\mathbb{R}^{\tilde{d}_k}$, and this is output as the node embedding $z_i = \tilde{h}_i^K$, with $K = 2$ indicating a two-layer graph convolutional network. These node embeddings are then incorporated into a multi-relational subgraph \tilde{G} , processed through a secondary two-layer graph convolutional network as shown in Equation(8) :

$$\tilde{h}_i^{k+1} = \sigma \left(\sum_{r \in \tilde{R}} \left(\sum_{j \in \tilde{N}_i^r} \frac{1}{\sqrt{|\tilde{N}_i^r| |\tilde{N}_j^r|}} \tilde{W}_r^k \tilde{h}_j^k + \frac{1}{|\tilde{N}_i^r|} \tilde{h}_i^k \right) \right) \quad (8)$$

In this expression, \tilde{R} represents the set of relation types in the second stage, \tilde{N}_i^r are the neighbors of v_i under relation r , and \tilde{W}_r^k is the layer-specific weight matrix corresponding to relation r in the second layer. This framework enables the encoding of higher-order neighborhood information, thereby enriching the representation of node features for downstream tasks. In this study, we improved upon the graph convolutional network encoder used by Yang et al[17]. to better suit our training data. Unlike the multi-relational subgraph approach mentioned in the previous model for the advanced node embedding process, we opted for a more direct method(Equation 9) to integrate the node embeddings of chemicals and genes:

$$h_i = h_i^C \oplus h_i^G \quad (9)$$

Here, h_i represents the final node embedding, with h_i^C and h_i^G respectively denoting the original embeddings of chemicals and genes. We merge these two types of node

embeddings through a simple vector concatenation operation \oplus , instead of the multi-subgraph structure mentioned in the previous model. This design choice is based on the characteristics and needs of our data, aiming to simplify the model structure while preserving key information. Our model utilizes the hierarchical structure of the graph convolutional network during the encoding phase, first calculating the embeddings for each type of node separately and then combining these embeddings through the concatenation operation. Such a structure allows the model to reduce computational complexity without sacrificing performance, enabling us to train on large-scale data.

7.0.2 Relational Graph Convolutional Network Tensor Decomposition

In this study, we introduce the Relational Graph Convolutional Network Tensor Decomposition (RGCNTD) decoder, which combines the Relational Graph Convolutional Network (RGCN) and Tensor Decomposition (TD). By superimposing a specially designed tensor decomposition layer on top of the graph convolutional layer, this model can capture and decode the complex relationships between entities more precisely. Our aim with this structural improvement is to enhance the model’s performance on multi-relational data prediction tasks. In the RGCNTD, we employ the Equation(10) to express the improved tensor decomposition layer.

$$Pred_{ij} = \sigma \left(\sum_{k=1}^K a_{ijk} \cdot (E_i \odot E_j \odot R_k) \right) \quad (10)$$

Here, $Pred_{ij}$ represents the predicted relational score between entity i and entity j , σ denotes a non-linear activation function, and \odot indicates the Hadamard product. E_i and E_j respectively represent the embeddings of the entities. Our RGCNTD takes the output of the RGCN layer as input for the tensor decomposition algorithm, using the graph structural features captured by the RGCN to enhance relation prediction. The update process of the RGCN layer is described by the following Equation(11):

$$H^{(l+1)} = \sigma \left(\sum_{r=1}^R \sum_{j \in N_i} \frac{1}{C_{ij}} W_r^{(l)} H_j^{(l)} \right) \quad (11)$$

$H^{(l+1)}$ denotes the entity embeddings at layer $l + 1$, R is the total number of relation types, N_i is the set of neighboring entities of entity i under relation r , c_{ij} is a normalization constant, $W_r^{(l)}$ is the weight matrix specific to the relation at layer l , and $H_j^{(l)}$ is the embedding of entity j at layer l . Within the RGCNTDDecoder, we employ a joint optimization strategy to train both the RGCN layer and the tensor decomposition layer simultaneously. The loss function Equation(12) is defined as the cross-entropy loss for the prediction of inter-entity relations, combined with a regularization term

to prevent overfitting:

$$\mathcal{L} = - \sum_{(i,j) \in \Omega} y_{ij} \log(\text{Pred}_{ij}) + (1 - y_{ij}) \log(1 - \text{Pred}_{ij}) + \lambda \|\theta\|^2 \quad (12)$$

Wherein, Ω is the set of all entity pairs in the training set, y_{ij} is the true label of the relationship between entity pair (i, j) , λ is the regularization parameter, and θ represents all parameters within the model. Through this joint optimization strategy, the model not only learns to extract effective feature representations from the graph structure, but also learns how to make accurate predictions of complex relationships through the tensor decomposition layer. This end-to-end training approach allows different parts of the model to interact and coordinate with each other, thereby improving the accuracy of predictions and the model’s generalization ability.

References

- [1] Pushpakom, S., Iorio, F., Eyers, P.A., Escott, K.J., Hopper, S., Wells, A., Doig, A., Guilleams, T., Latimer, J., McNamee, C., *et al.*: Drug repurposing: progress, challenges and recommendations. *Nature reviews Drug discovery* **18**(1), 41–58 (2019)
- [2] Abdulaziz, L., Elhadi, E., Abdallah, E.A., Alnoor, F.A., Yousef, B.A.: Antiviral activity of approved antibacterial, antifungal, antiprotozoal and anthelmintic drugs: Chances for drug repurposing for antiviral drug discovery. *Journal of experimental pharmacology*, 97–115 (2022)
- [3] Ali, I., A Wani, W., Saleem, K., Haque, A.: Thalidomide: A banned drug resurged into future anticancer drug. *Current drug therapy* **7**(1), 13–23 (2012)
- [4] Anda-Jáuregui, G., Guo, K., McGregor, B.A., Hur, J.: Exploration of the anti-inflammatory drug space through network pharmacology: applications for drug repurposing. *Frontiers in Physiology* **9**, 309929 (2018)
- [5] Hopkins, A.L.: Network pharmacology: the next paradigm in drug discovery. *Nature chemical biology* **4**(11), 682–690 (2008)
- [6] Zimmermann, G.R., Lehar, J., Keith, C.T.: Multi-target therapeutics: when the whole is greater than the sum of the parts. *Drug discovery today* **12**(1-2), 34–42 (2007)
- [7] Crichton, G., Guo, Y., Pyysalo, S., Korhonen, A.: Neural networks for link prediction in realistic biomedical graphs: a multi-dimensional evaluation of graph embedding-based approaches. *BMC bioinformatics* **19**, 1–11 (2018)
- [8] Zemouri, R., Zerhouni, N., Racoceanu, D.: Deep learning in the biomedical applications: Recent and future status. *Applied Sciences* **9**(8), 1526 (2019)

- [9] Sosa, D.N., Derry, A., Guo, M., Wei, E., Brinton, C., Altman, R.B.: A literature-based knowledge graph embedding method for identifying drug repurposing opportunities in rare diseases. In: Pacific Symposium on Biocomputing 2020, pp. 463–474 (2019). World Scientific
- [10] Gaudelet, T., Day, B., Jamasb, A.R., Soman, J., Regep, C., Liu, G., Hayter, J.B., Vickers, R., Roberts, C., Tang, J., *et al.*: Utilizing graph machine learning within drug discovery and development. *Briefings in bioinformatics* **22**(6), 159 (2021)
- [11] Zitnik, M., Agrawal, M., Leskovec, J.: Modeling polypharmacy side effects with graph convolutional networks. *Bioinformatics* **34**(13), 457–466 (2018)
- [12] Cotto, K.C., Wagner, A.H., Feng, Y.-Y., Kiwala, S., Coffman, A.C., Spies, G., Wollam, A., Spies, N.C., Griffith, O.L., Griffith, M.: Dgidb 3.0: a redesign and expansion of the drug–gene interaction database. *Nucleic acids research* **46**(D1), 1068–1073 (2018)
- [13] Du, M., Ma, B., Meng, D.: Edge convergence problems on signed networks. *IEEE transactions on cybernetics* **49**(11), 4029–4041 (2018)
- [14] Derr, T., Ma, Y., Tang, J.: Signed graph convolutional networks. In: 2018 IEEE International Conference on Data Mining (ICDM), pp. 929–934 (2018). IEEE
- [15] Yang, F., Fan, K., Song, D., Lin, H.: Graph-based prediction of protein-protein interactions with attributed signed graph embedding. *BMC bioinformatics* **21**, 1–16 (2020)
- [16] Mason, M.J., Fan, G., Plath, K., Zhou, Q., Horvath, S.: Signed weighted gene co-expression network analysis of transcriptional regulation in murine embryonic stem cells. *BMC genomics* **10**, 1–25 (2009)
- [17] Yang, F., Fan, K., Song, D., Lin, H.: Graph-based prediction of protein-protein interactions with attributed signed graph embedding. *BMC bioinformatics* **21**, 1–16 (2020)
- [18] Chen, M., Jiang, W., Pan, Y., Dai, J., Lei, Y., Ji, C.: Sgfnns: Signed graph filtering-based neural networks for predicting drug–drug interactions. *Journal of Computational Biology* **29**(10), 1104–1116 (2022)
- [19] Kuhn, M., Mering, C., Campillos, M., Jensen, L.J., Bork, P.: Stitch: interaction networks of chemicals and proteins. *Nucleic acids research* **36**(suppl_1), 684–688 (2007)
- [20] Li, Y., Xiong, H., Kong, L., Wang, S., Sun, Z., Chen, H., Chen, G., Yin, D.: Ltrgcn: Large-scale graph convolutional networks-based learning to rank for web search. In: Joint European Conference on Machine Learning and Knowledge Discovery in Databases, pp. 635–651 (2023). Springer

- [21] Yang, X., Wang, W., Ma, J.-L., Qiu, Y.-L., Lu, K., Cao, D.-S., Wu, C.-K.: Bionet: a large-scale and heterogeneous biological network model for interaction prediction with graph convolution. *Briefings in bioinformatics* **23**(1), 491 (2022)
- [22] Wang, Y., Xiao, J., Suzek, T.O., Zhang, J., Wang, J., Bryant, S.H.: Pubchem: a public information system for analyzing bioactivities of small molecules. *Nucleic acids research* **37**(suppl_2), 623–633 (2009)
- [23] Degtyarenko, K., De Matos, P., Ennis, M., Hastings, J., Zbinden, M., McNaught, A., Alcántara, R., Darsow, M., Guedj, M., Ashburner, M.: ChEBI: a database and ontology for chemical entities of biological interest. *Nucleic acids research* **36**(suppl_1), 344–350 (2007)
- [24] Coudert, E., Gehant, S., Castro, E., Pozzato, M., Baratin, D., Neto, T., Sigrist, C.J., Redaschi, N., Bridge, A.: Annotation of biologically relevant ligands in uniprotkb using chebi. *Bioinformatics* **39**(1), 793 (2023)
- [25] Mering, C.v., Huynen, M., Jaeggi, D., Schmidt, S., Bork, P., Snel, B.: STRING: a database of predicted functional associations between proteins. *Nucleic acids research* **31**(1), 258–261 (2003)
- [26] Zhang, Z., Li, M., Lin, X., Wang, Y.: Network-wide traffic flow estimation with insufficient volume detection and crowdsourcing data. *Transportation Research Part C: Emerging Technologies* **121**, 102870 (2020)